scientific reports

OPEN

Study on particle deposition and flow characteristics of edible chili oil in bending pipe conveyance in industrial production

Jiacheng Zhuang[1], Qiushi Shi[2] & Zhi Han[2]✉

This study develops a coupled computational fluid dynamics (CFD) and discrete element method (DEM) two-phase flow model to investigate particle deposition behaviors in industrial pipeline transportation of edible chili oil, a high-viscosity fluid widely used in food industries. Due to its complex rheological properties and the presence of suspended solids, chili oil pipelines frequently face significant challenges, including excessive particle deposition at pipe bends, increased pressure drops, and energy inefficiency. To address these critical issues, simulations were systematically conducted using the Realizable k-ε turbulence model, examining the effects of different inlet velocities (0.5–2.5 m/s), particle sizes (2–4 mm), and particle shapes (spherical, rod-shaped, and cubic). Results showed that operating the pipeline within an optimal transport velocity range of approximately 1.0–1.5 m/s effectively minimized particle accumulation at bends and significantly reduced pressure losses. Quantitatively, spherical particles exhibited the lowest pressure drop increase (from approximately 3.45 kPa at 0.5 m/s to 21.78 kPa at 2.5 m/s) due to reduced collision frequencies and kinetic energy dissipation. In contrast, irregular particles (cubic shapes) led to the highest pressure drops, rising sharply from 5.91 kPa at 0.5 m/s up to 34.56 kPa at 2.5 m/s, caused by frequent collisions and turbulent fluctuations. Additionally, simulations revealed that increasing particle size from 2 to 4 mm notably decreased particle deposition and pressure losses due to reduced collision frequency and enhanced momentum transfer. These quantitative findings not only fill the research gap concerning high-viscosity, particulate-laden edible fluid systems but also provide concrete and practical guidelines for optimizing chili oil transport processes. The findings directly contribute to improved operational reliability, lower energy consumption, and reduced blockage risks in industrial food pipeline applications.

The transportation of particulate-laden fluids through pipelines is a crucial operation in various industrial processes, particularly in food and beverage production, where the control of deposition behavior plays a pivotal role in both efficiency and quality. Among these processes, the transport of edible chili oil is of notable interest due to its complex rheological properties and the challenges associated with particle deposition during conveyance. Chili oil, commonly used in culinary applications, is a high-viscosity fluid with changing characteristics, presenting challenges to flow dynamics and deposition patterns in pipeline systems. The deposition of particulate matter, particularly within bends of pipelines, can significantly influence system performance, leading to blockages, reduced flow efficiency, and potential contamination risks. Therefore, understanding the particle–fluid interactions and the factors influencing deposition is critical for optimizing the transportation system in the food industry.

Computational fluid dynamics (CFD) coupled with discrete element method (DEM) simulations have emerged as a powerful tool for investigating such complex fluid-particle systems. CFD provides detailed insights into fluid flow, while DEM simulates particle behavior, including interactions with both fluids and other particles[1–4]. The combination of these two methods allows for a more comprehensive understanding of the dynamics governing particle deposition and its dependence on key factors such as particle size, shape, and the flow characteristics of

[1]Research Center of Fluid Machinery Engineering and Technology, Jiangsu University, Zhenjiang 212013, China. [2]School of Energy and Power Engineering, Jiangsu University, Zhenjiang 212013, China. ✉email: hands@ujs.edu.cn

the fluid. Numerous studies have applied CFD-DEM simulations to model particle deposition in different flow systems, with a significant body of work focusing on applications in industrial pipelines[5–7].

In the context of edible chili oil, its rheological behavior influences both the flow regime and the particle deposition process. The interaction between the viscous forces of the chili oil and the inertial forces of the particles in the flow must be carefully considered to accurately predict deposition patterns. Research on chili oil flow, especially in the food industry, remains limited and often focuses on idealized conditions such as steady flow or uniform particle sizes[8]. In contrast, real-world industrial systems often exhibit more variability, with irregular particle shapes, a wide range of particle sizes, and fluctuating flow rates, which necessitate more sophisticated modeling techniques.

Numerical simulation methods can provide sufficient detail on the flow behavior of transported materials under various conditions. Hence, the CFD-DEM computational model can be applied to the pipeline transportation processes[9]. This approach can effectively capture the influence of particle physical characteristics on the flow of solid–liquid mixtures. Bilal et al. demonstrated that under constant flow rates, particles with large aspect ratios exhibit stronger interaction forces both between particles and with the pipe wall[10]. Chen et al.[11], Uzi et al.[12], and Zhou et al.[13] established the influence of the variation of solid–liquid interaction forces on two-phase systems in horizontal pipelines for different material conditions on concentration and velocity distributions and, ultimately, the flow characteristics of two-phase systems. In addition, Dai et al.[14] investigated the motion characteristics under varying flow velocities and particle concentrations in a vertical pipeline. However, most of these studies have focused solely on a single-particle size, neglecting the effects of different particle shapes. CFD-DEM method, an effective approach to handling two-phase flow problems, is an important means in solid–liquid interaction numerical simulation[15–17]. In this regard, Peng et al.[18] have explored the characteristics of liquid–solid flow in modified fluidized beds with an inclined channel to find out the optimum flow rates.

Furthermore, although particle deposition at pipe bends has been extensively studied in simplified systems, fluids containing irregularly shaped and polydisperse particles remain underexplored[19]. Research on the deposition mechanisms of such fluids in pipe bends is scarce, and there is a need to examine the influence of flow velocity, pipe geometry, and particle characteristics on the deposition process[20–23]. Previous studies have demonstrated that factors such as particle shape (spherical vs. non-spherical), flow rate, and pipe geometry (curvature and bend angle) can significantly alter deposition patterns[24]. However, these findings often lack detailed experimental validation and real-world applicability, particularly in the case of high-viscosity food-grade fluids[25].

This study aims to bridge this gap by investigating the deposition behavior and flow characteristics of edible chili oil in industrial pipeline conveyance, focusing on bends where deposition is most likely to occur. Using a CFD-DEM coupled approach, the study examines the influences of flow velocity, particle size, and shape on particle deposition in a bending pipe system[26]. Additionlly, it delves into the rheological properties of chili oil, including its shear-thinning behavior and yield stress, which are critical for accurately simulating fluid-particle interactions. The model is validated against available experimental data in the literature, and the results are analyzed to provide practical guidelines for optimizing chili oil transport in industrial systems. This paper presents a comprehensive exploration of the particle deposition process, providing valuable insights for the food industry and offering a solid foundation for future studies in industrial fluid transport systems.

By addressing the complex dynamics of particle-laden flow in pipeline bends, this research contributes not only to the academic understanding of particle deposition but also to practical improvements in the efficiency and reliability of chili oil transportation in industrial settings. The findings are expected to have broader applications in the food processing industry, where similar challenges in particle transport and deposition are encountered. Through this work, we seek to contribute to the optimization of industrial pipeline systems and improve chili oil production processes, with the potential to enhance both operational efficiency and product safety.

Materials and method
Mathematical model
During the pipeline transportation of a chili oil-based solid–liquid two-phase flow, the system behavior follows the fundamental principles of fluid dynamics and is governed by three conservation laws: conservation of mass, momentum and energy. In fluid mechanics, these laws correspond to the continuity equation, the Navier–Stokes equations and the Bernoulli equation, respectively. Together, these equations form the mathematical basis for analyzing flow characteristics.

The governing equations become particularly complex and variable because the liquid phase behaves as a non-Newtonian fluid. Analytical solutions are often intractable and insufficiently accurate for such complex flow conditions. Therefore, experimental studies usually depend on computational techniques to simulate the motion of this fluid and get approximate solutions. Computer simulations enhance both computational efficiency and accuracy while providing intuitive visualizations to observe flow phenomena. This is important for revealing physical phenomena in complex flow fields and identifying critical parameters for engineering applications.

In this study, the Realizable k-ε turbulence model was used, incorporating the interaction forces between particles. A CFD-DEM coupling model for horizontal solid–liquid two-phase flow was developed. Using this model, the influences of different initial velocities, particle sizes and particle shapes on hydraulic transport in a 90° bend were investigated.

Governing equations of fluid flow
In fluid mechanics, when considering interactions between fluids and particles, the fluid is typically treated as the continuous phase, while the particles are regarded as the dispersed phase. The motion of the continuous phase fluid is governed by the laws of mass and momentum conservation. The volume-averaged and Reynolds-averaged continuity and momentum equations for the fluid are as follows:

$$\frac{\partial}{\partial t}(\alpha_f \rho_f) + \nabla \cdot (\alpha_f \rho_f \overline{v}_f) = 0 \tag{1}$$

$$\frac{\partial}{\partial t}(\alpha_f \rho_f \overline{v}_f) + \nabla \cdot (\alpha_f \rho_f \overline{v}_f \overline{v}_f) = -\nabla p$$
$$+ \nabla \cdot \left[\alpha_f (\mu_f + \mu_t) \left(\nabla \overline{v}_f + \nabla \overline{v}_f^T \right) \right] + \alpha_f \rho_f + F_{p-f} \tag{2}$$

where $\rho_f, \alpha_f, \mu_f, \mu_t, \overline{v}_f$ represent the fluid density (kg/m³), fluid volume fraction (%), fluid dynamic viscosity (Pa s), fluid turbulent viscosity (Pa s), and average fluid velocity (m/s), respectively. Additionally t, p, and g denote time (s), pressure (Pa), and gravitational acceleration (m/s²), respectively. The term F$_{p-f}$ represents the force source term exerted by the particles on the fluid (N/m³). To account for the influence of particles on the fluid, a source term is incorporated into the momentum equation, expressed as follows:

$$F_{p-f} = -\frac{1}{V_{cell}} \sum_{i=1}^{n} F_{f-p} \tag{3}$$

In Eq. (3), V_{cell} and F_{f-p} represent the volume of the fluid mesh (m³) and the total force exerted by the fluid on the particles (N), respectively, while n indicates the number of particles within the fluid mesh.

In solid–liquid two-phase flow, the presence of the dispersed phase influences both the enhancement and attenuation of turbulence. To account for this influence, a turbulence source term is incorporated into the model to reflect the influence of particles on turbulence[27]:

$$S_k = \frac{1}{V_{cell}} \sum_{i=1}^{n} 3\pi \mu_f d_i f_i |v_f - v_i|^2 \tag{4}$$

$$S_\varepsilon = \rho_f C'_{\varepsilon 3} \frac{\nu_f^2}{V_{cell}} \sum_{i=1}^{n} f_i \frac{|v_f - v_i|^2}{d_i} \tag{5}$$

In this context, S_k and S_ε denote the turbulence kinetic energy source term and the turbulence dissipation source term, respectively. v_f represents the instantaneous velocity of the fluid, while v_f and v_f refer to the velocity and diameter of particle iii, respectively. f_i and $C'_{\varepsilon 3}$ are coefficients associated with the particle Re. Additionally, n indicates the number of particles within the fluid mesh, and v_f signifies the dynamic viscosity of the fluid.

Particle motion equations

In this study, particle motion is modeled using the Discrete Element Method (DEM), which describes particle dynamics according to Newton's second law:

$$m_i \frac{dv_i}{dt} = F_{g,i} + F_{f-p,i} + \sum_{j=1, j \neq i}^{k_c} F_{c,ij} \tag{6}$$

$$I_i \frac{d\omega_i}{dt} = \sum_{j=1, j \neq i}^{k_c} (T_{c,ij} + T_{r,ij}) + T_{f,i} \tag{7}$$

$$F_{f-p,i} = F_{drag,i} + F_{lift,i} + F_{p,i} + F_{vm,i} \tag{8}$$

$$T_{c,ij} = r_i \times F_{ct,ij} \tag{9}$$

$$T_{r,ij} = -\mu_s F_{cn,ij} r_i \Omega_i \tag{10}$$

where, m_i denotes the mass of the particle; F$_{g,i}$ represents the gravitational force; $F_{f-p,i}$ is the total force exerted by the fluid on the particle, including interactions from particles or walls; $F_{drag,i}$ indicates the drag force; $F_{lift,i}$ represents the lift force; $F_{p,i}$ is the pressure gradient force; $F_{vm,i}$ denotes the virtual mass force; k_c indicates the total number of contacts between particle; I_i represents the moment of inertia (kg·m³); ω_i is the angular velocity (s⁻¹); $T_{c,ij}$ denotes the torque due to tangential forces between particles; $T_{r,ij}$ represents the rolling friction torque; $T_{f,i}$ is the torque exerted by the fluid; $T_{cn,ij}$ denotes the normal contact force; $F_{ct,ij}$ is the tangential contact force; r_i is the distance vector from the particle's center of mass to the contact point; μ_s is the rolling friction coefficient; r$_i$ represents the distance from the particle's center of mass to the contact point; and Ω_i is the unit vector representing the direction at the contact point.

Fluid-particle interaction forces

This section presents the motion equations for particles in a liquid, along with the implementation of numerical simulations. Compared to the Eulerian-Lagrange method, the Eulerian-Eulerian method yields satisfactory results in studying turbulent flows containing particles, while offering greater efficiency[28].

Fluid phase[29]:

$$\nabla \times (-\alpha_f \rho_f \vec{v}_f \vec{v}_f) = -\alpha_f \nabla P + \nabla \cdot \bar{\bar{\tau}}_f + \alpha_f \rho_f \vec{g} + K_{sf}(\vec{v}_s - \vec{v}_f)$$
$$+ C_{vm}\alpha_f \rho_f (\vec{v}_s \nabla \vec{v}_s - \vec{v}_f \nabla \vec{v}_f) + C_L \alpha_s \rho_f (\vec{v}_f - \vec{v}_s) \times (\nabla \times \vec{v}_f) \tag{11}$$

Solid Phase:

$$\nabla \times (\alpha_s \rho_s \vec{v}_s \vec{v}_s) = -\alpha_s \nabla P - \nabla P_s + \nabla \cdot \bar{\bar{\tau}}_s + \alpha_s \rho_f \vec{g} + K_{fs}(\vec{v}_f - \vec{v}_s)$$
$$+ C_{vm}\alpha_s \rho_f (\vec{v}_f \nabla \vec{v}_f - \vec{v}_s \nabla \vec{v}_s) + C_L \alpha_s \rho_f (\vec{v}_s - \vec{v}_f) \times (\nabla \times \vec{v}_f) \tag{12}$$

where $\bar{\bar{\tau}}_f$ and $\bar{\bar{\tau}}_s$ represent the stress tensors for the solid and fluid phases, respectively; α_f and α_s denote the volume fractions of the fluid and solid phases; ∇P indicates the static pressure gradient; ∇P_s represents the pressure gradient in the solid phase or the inertial forces arising from particle interactions; K_{sf} is the interphase drag coefficient; $\vec{v}_s$ and $\bar{\bar{\tau}}_f$ are the velocities of the solid and liquid phases, respectively; and $\bar{\bar{\tau}}_f$ signifies the stress tensor of the fluid.

When relative motion occurs between the fluid and solid particles, momentum transfer is initiated. The surface of the particles exerts a drag force on the fluid, while the fluid applies a lift force on the particle surfaces. These drag and lift forces represent an action-reaction pair:

$$F_d = F_\tau + F_P = 4\pi\mu Ru + 2\pi\mu Ru = 6\pi\mu Ru \tag{13}$$

$$\mathrm{Re}_p = \frac{d_p u \rho}{\mu} \tag{14}$$

where F_d represents the total drag force on the particle surface:

$$F_d = C_D A_P \frac{\rho u^2}{2} \tag{15}$$

Particle modeling and material properties

To comprehensively investigate the flow behavior in pipe transportation under diverse conditions, simulations were carried out on bends with a radius-to-diameter ratio of three, exploring different inlet initial velocities and particle sizes. For non-spherical particles, all other physical properties (e.g., density, surface roughness) were kept identical to those of spherical particles to isolate the effect of shape on flow behavior. Non-spherical particles were constructed by close-packing assemblies of multiple spherical units through an inscribed filling method. Cylindrical particles: Composed of 4 standard spheres (diameter = 0.8 mm) arranged linearly, achieving an aspect ratio of 3:1 (length-to-diameter). Square-shaped particles: Formed by 27 standard spheres (diameter = 1.4 mm) arranged in a $3 \times 3 \times 3$ cubic lattice, yielding a cubic structure with edge length = 3.24 mm. The geometric configurations of these particles are illustrated in Fig. 1.

Numerical simulation setup

To analyze the motion of solid particles in the oil phase, CFD-DEM coupling was adopted. In this study, the oil in chili oil was modeled as the liquid phase, and the particles as the solid phase. The liquid phase was modeled as a continuous medium. Therefore, the Realizable k-ε turbulence model was employed. The governing equations for turbulence kinetic energy K and dissipation ε are as follows:

$$\frac{\partial}{\partial t}(\rho k) + \frac{\partial}{\partial x_i}(\rho k u_i) = \frac{\partial}{\partial x_j}\left[\left(\mu + \frac{\mu_t}{\sigma_k}\right)\frac{\partial k}{\partial x_j}\right] + G_k + G_b - \rho\varepsilon - Y_M \tag{16}$$

$$\frac{\partial}{\partial t}(\rho\varepsilon) + \frac{\partial}{\partial x_i}(\rho\varepsilon u_i) = \frac{\partial}{\partial x_j}\left[\left(\mu + \frac{\mu_t}{\sigma_\varepsilon}\right)\frac{\partial\varepsilon}{\partial x_j}\right] + C_{1\varepsilon}\frac{\varepsilon}{k}(G_k + G_{3\varepsilon}G_b) - G_{2\varepsilon}\rho\frac{\varepsilon^2}{k} - R_\varepsilon \tag{17}$$

In this context, $C_{1\varepsilon} = 1.42$、$G_{2\varepsilon} = 1.92$、$C_\mu = 0.009$, where ρ denotes the density of the liquid. The Prandtl numbers for turbulent kinetic energy k and the rate of turbulent energy dissipation ε are set at $\sigma_k = 1.0$ and
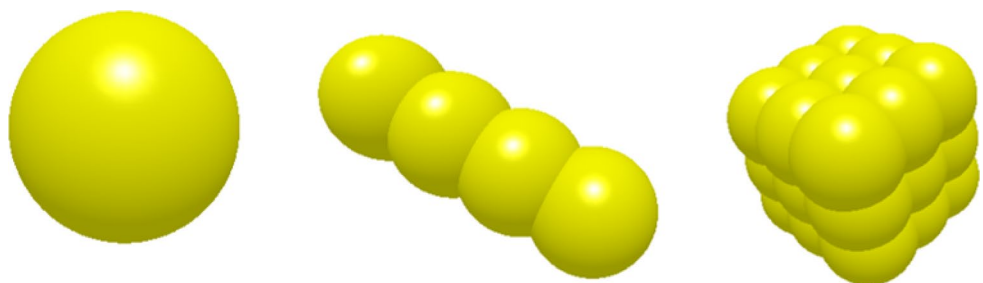

Fig. 1. Spherical particles, rod-shaped particles, cubic particles.

$\sigma_\varepsilon = 1.3$, respectively. μ_t represents the effective viscosity coefficient $\mu_t = \rho C_\mu \frac{k^2}{\varepsilon}$; G_k signifies the turbulent kinetic energy generated by the average velocity gradient. G_b refers to the turbulent kinetic energy arising from buoyancy, and Y_M accounts for the fluctuations induced by transitional diffusion. $C_{3\varepsilon}$ is a constant in the equation, and R_ε is an additional source term included in the formulation.

Furthermore, the settling velocity at the end of the pipeline is critical in determining whether particles will deposit. In this work, the Delft head loss and limit settling velocity (DHLLDV) framework was utilized, which has been refined multiple times by Miedema et al.[30]. The DHLLDV framework describes the hydraulic gradient curve for spatial volume concentration and uniform sand, encompassing all flow regimes associated with the pipeline and the relevant particle diameters. The velocity at this point is defined as the limit static settling velocity (LSDV) and is calculated via Eq. (18):

$$V_{ls.fs}^2 = \frac{2 \times \mu_{sf} \times g \times C_{vs} \times R_{sd}}{\frac{\lambda_r}{D_H} \times \left(\frac{A_P}{A_H}\right)^2 - \frac{\lambda_l}{D_P}} \tag{18}$$

where A_P represents the cross-sectional area of the pipe, A_H is the cross-sectional area of the restricted zone above the particle bed, μ_{sf} is the coefficient of sliding friction, C_{vs} denotes the spatial volume concentration, and R_{sd} indicates the relative underwater density. Additionally, λ_r is the Darcy-Weisbach friction factor for the restricted zone above the particle bed, λ_r is the Darcy-Weisbach friction factor between the liquid and the pipe wall, D_H represents the hydraulic diameter of the cross-section above the particle bed, and D_P is the diameter of the pipe.

In Fluent, the Realizable k-ε model was employed for the simulations. The inlet boundary condition was set as a velocity inlet, while the outlet boundary condition was specified as a pressure outlet. The simulation time step in Fluent was configured to 1×10^{-3} s, with a convergence criterion of 10^{-4}. In EDEM, the Hertz-Mindlin (epsilon) model was chosen for particle collisions. The time step in EDEM is typically smaller than that in Fluent and must be an integer multiple of the Fluent time step, ensuring the Rayleigh time is approximately 20%. Consequently, the time step for the bend in EDEM was set at 5×10^{-6} s. This study focuses on chili oil, with solid particles modeled in EDEM. The spherical particles were scaled to resemble sesame seeds, with diameters of 2, 3, and 4 mm. Additionally, various particle shapes were considered based on practical relevance. Irregular particles were created by combining multiple spherical units within a defined space. Rod-shaped particles were modeled by arranging four standard spheres (diameter 0.8 mm) sequentially to form a total length of 2.3 mm. Square particles were constructed by assembling 27 spheres, each with a diameter of 1.4 mm, into a cuboid measuring 3.24 mm in length, width, and height. Table 1 summarizes the numerical values of the relevant simulation parameters.

Geometrical model and dimensions
The numerical simulation pipeline model was constructed and meshed using ICEM. The internal diameter of the bend was set to D = 100 mm, with a straight pipe length of L = 1000 mm and a bend radius of R = 3D. The gravitational force was applied along the negative y-axis direction. Monitoring points were set up every 20 mm along the curved section. The geometric model is shown in Fig. 2.

Mesh generation and independence verification
The fluid domain pipeline model was meshed using ICEM. To enhance mesh quality, an "O-grid" partitioning was applied to the circular cross-section of the pipeline. The overall mesh quality exceeded 0.4, and grids with quantities of 33,075, 49,031, 64,827, 81,024, 95,985, 109,561, and 124,758 were generated for grid independence verification. By collecting and comparing velocities at the bend outlet (results shown in Fig. 3), the data stabilized when the grid count exceeded 5×10^4. Considering the large particle size and the influence of total particle volume fraction in this study, the grid number and size were constrained to balance computational accuracy and efficiency in Fluent. Consequently, a grid count of 6.5×10^4 was selected for simulations.

Parameters	Numerical value
Solid DENSITY (kg/m³)	930
Liquid density (kg/m³)	900
Poisson's ratio	0.481
Shear Modulus (Pa)	2.495×10^6
Particle–particle coefficient of restitution	0.278
Particle–particle static friction coefficient	0.57
Particle–particle dynamic friction coefficient	0.01
Particle-PVC coefficient of restitution	0.36
Particle-PVC static friction coefficient	0.49
Particle-PVC dynamic friction coefficient	0.03

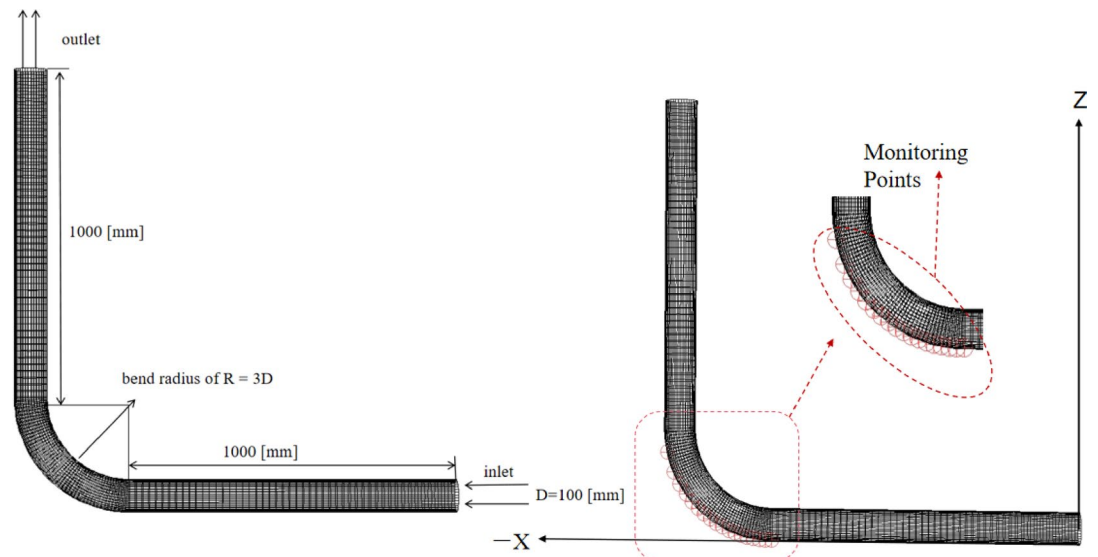**Table 1.** Simulation parameters.
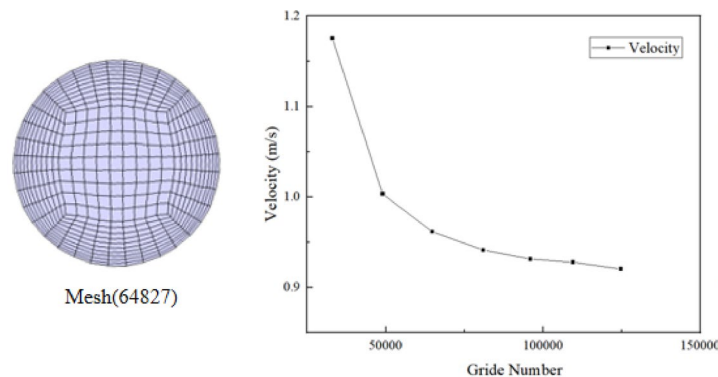
Fig. 2. Pipe geometry.

Fig. 3. Grid quantity and independence verification.

Model validation

To validate the accuracy of the model, a water-only flow model with a velocity of 3.56 m/s was simulated and compared against results from the literature[31]. Figure 4 demonstrates the validation of the CFD-DEM fully coupled model. As shown, the model results accurately predict the pressure fitting function from the literature, aligning well with the trend of the fitted curve reported in the literature. The errors in the results are all below 8%. The deviation is primarily attributed to differences in boundary conditions and the simplifications inherent in the numerical model. This level of error is considered acceptable in the context of multiphase CFD-DEM simulations. It is also noted that no experimental validation was conducted in this study. Future work will aim to incorporate experimental comparisons to further validate and enhance model accuracy.

Results and discussion
Influence of initial velocity on flow

Under the constant condition of an inflow particle volume fraction of 10%, gravity was oriented along the negative Y-axis to accurately reflect real-world conditions. To comprehensively analyze the hydrodynamic characteristics within the bend under different flow velocities, three inlet initial velocities were defined: 0.5 m/s, 1 m/s, and 1.5 m/s. This configuration aims to systematically investigate the influence of flow velocity variations on particle flow patterns in the bend.

As clearly illustrated in Fig. 5, the numerical simulation results reveal significant differences in particle flow behavior under gravity as the inlet velocity increases. At 0.5 m/s, due to the relatively low flow velocity, the average velocity stabilizes at 0.32 m/s after reaching steady-state flow. In the bend region, particularly near the inner curvature, a continuous particle deposition band with a thickness of 8.4 mm forms, highlighting the dominant role of gravity in particle sedimentation under low-speed conditions. When the inlet velocity increases to 1 m/s, particle deposition near the inner bend weakens, indicating enhanced particle transport capacity at higher velocities. At 1.5 m/s, the deposition thickness further reduces to 1.8 mm. However, the stabilized average
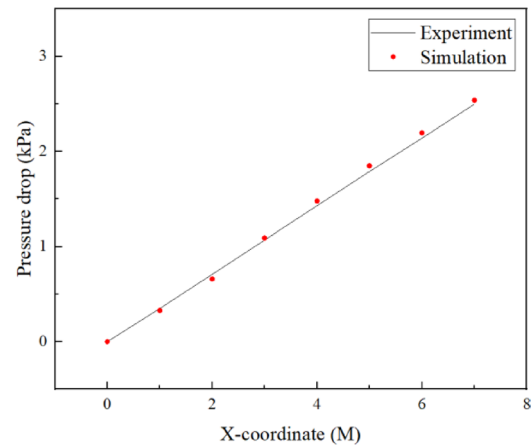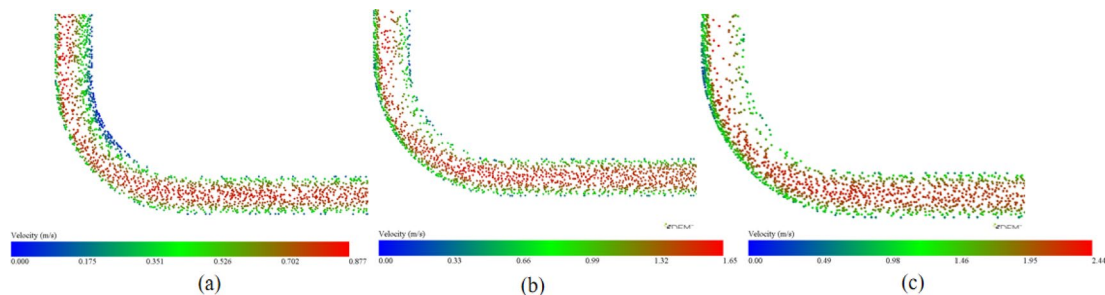
Fig. 4. Model validation.

Fig. 5. Particle motion states in the pipeline under different initial velocities: (**a**) 0.5 m/s; (**b**) 1.0 m/s; (**c**) 1.5 m/s.

Inlet initial velocity (m/s)	Inner bend deposition thickness (mm)	Pipeline pressure drop ΔP (kPa)	Average flow velocity (m/s)	Steady-state kinetic energy value (J)
0.5	8.4	0.6	0.32	8.8×10^{-6}
1.0	5.2	1.2	0.79	3.3×10^{-5}
1.5	1.8	3.5	1.05	7.3×10^{-5}

Table 2. Bend pipe flow parameter comparison.

velocity rises to 1.05 m/s (Table 2), where intensified particle–wall friction due to high-speed flow not only decelerates particles but also induces new deposition phenomena. This underscores the critical influence of particle–wall interactions on hydrodynamics in high-velocity regimes.

For an in-depth analysis of hydrodynamic characteristics, Fig. 7a,b present the temporal evolution of kinetic energy and velocity at the bend cross-section. For the 1.5 m/s case, the kinetic energy rapidly peaks at 9.4×10^{-5} J within the initial $0 \sim 1$ s, then stabilizes at 7.3×10^{-5} J due to energy dissipation against flow resistance. In contrast, the 0.5 m/s case shows a lower peak kinetic energy of 1.2×10^{-5} J, stabilizing at 8.8×10^{-6} J. Comparatively, the 0.5 m/s case exhibits a reduced average velocity (from 1.05 to 0.15 m/s), increased inner bend deposition thickness (from 1.8 to 8.4 mm), and a pressure drop rise to 0.6 kPa (Fig. 6). These findings elucidate the energy conversion and velocity distribution in the bend, offering critical data for understanding curved-pipe flow behavior.

For Fig. 7c,d, the data were collected from dynamic and static pressure monitoring points positioned at 20 mm intervals along the bend wall, starting from the 1000 mm position. A significant positive correlation was observed between dynamic pressure and velocity:

$$P = \frac{\rho v^2}{2}$$ (19)

Given that the solid–liquid phase density remains constant in this study, variations in dynamic pressure align consistently with fluctuations in particle velocity. This finding holds profound implications for elucidating the
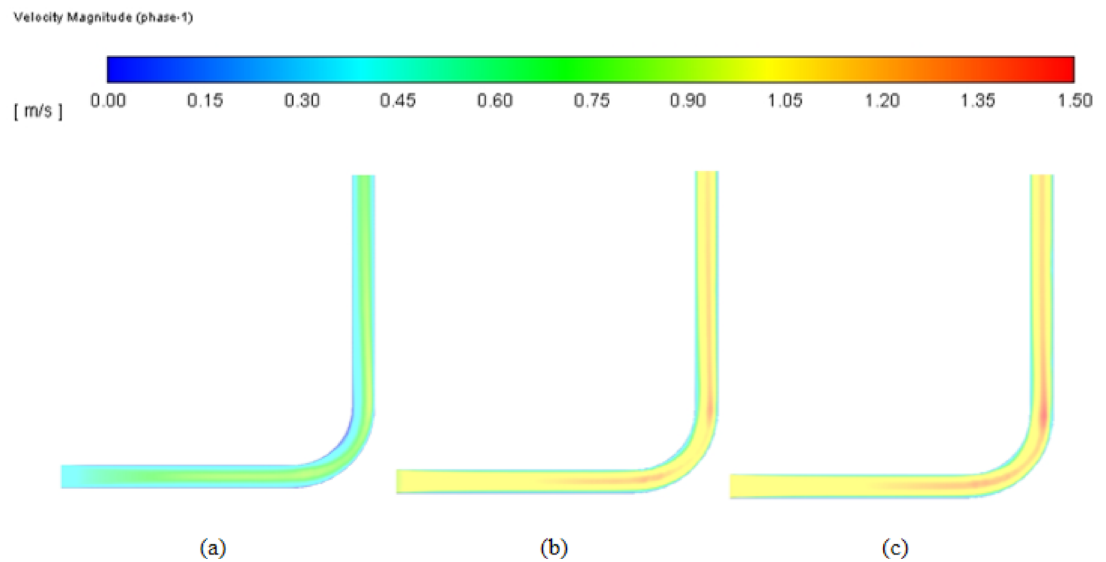
Fig. 6. Steady-state flow velocity in pipelines under different initial velocities: (a) 0.5 m/s; (b) 1.0 m/s; (c) 1.5 m/s.
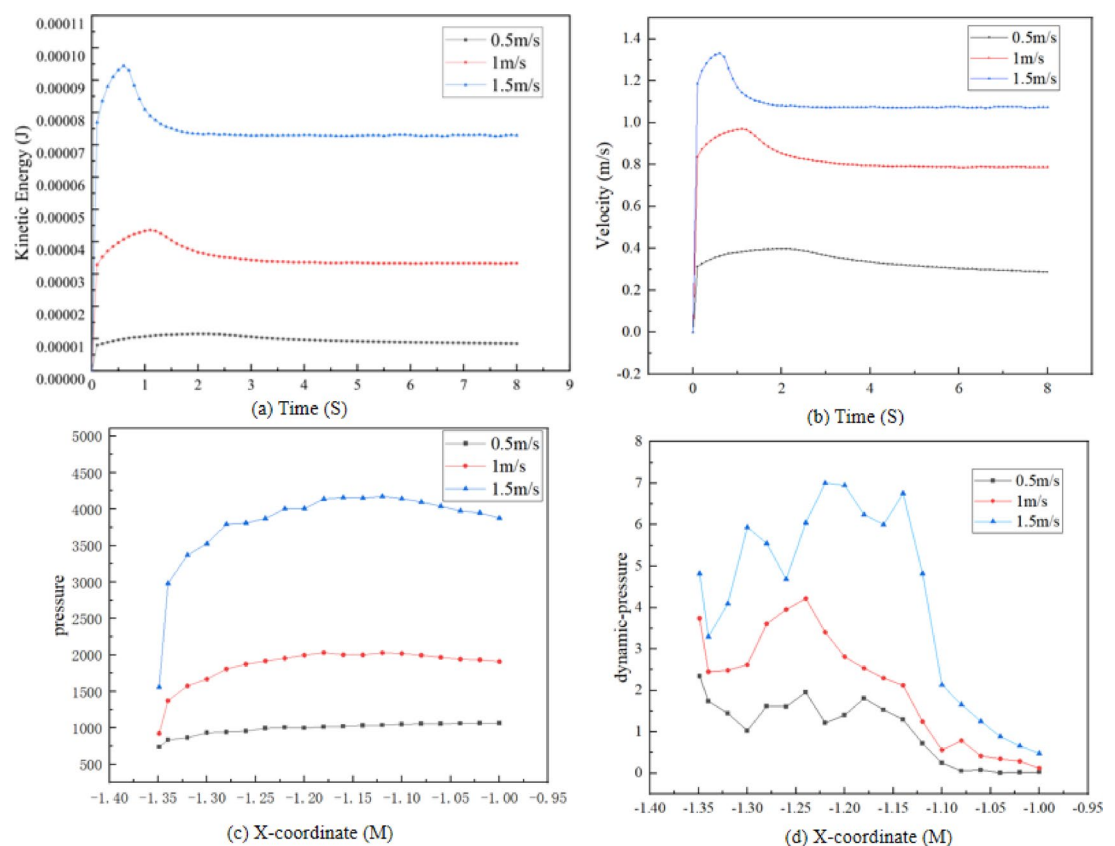

Fig. 7. (a) Kinetic energy versu time; (b) Velocity versus time; (c) Pressure versus position; (d) Dynamic pressure versus position.

motion mechanisms of particles within the fluid. It is worth noting that, unless otherwise specified, the term "pressure" in this study refers to static pressure.

In Fig. 7c,d, the straight pipe segment exhibits relatively high pressure due to gravitational acceleration. However, pressure distribution undergoes significant changes in the bend region. At low velocities, the outer bend shows lower pressure due to centrifugal force-driven fluid migration toward the outer wall, reducing
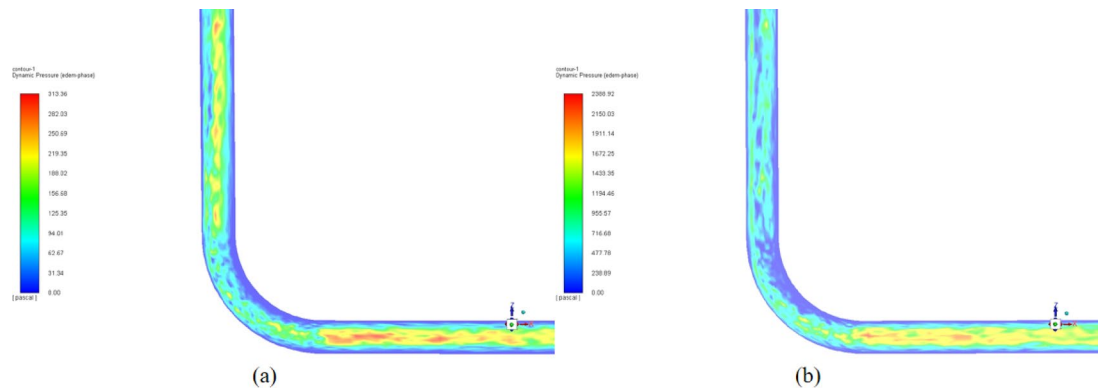
Fig. 8. Pressure contour plots at bend center for 0.5 m/s and 1.5 m/s initial velocities.
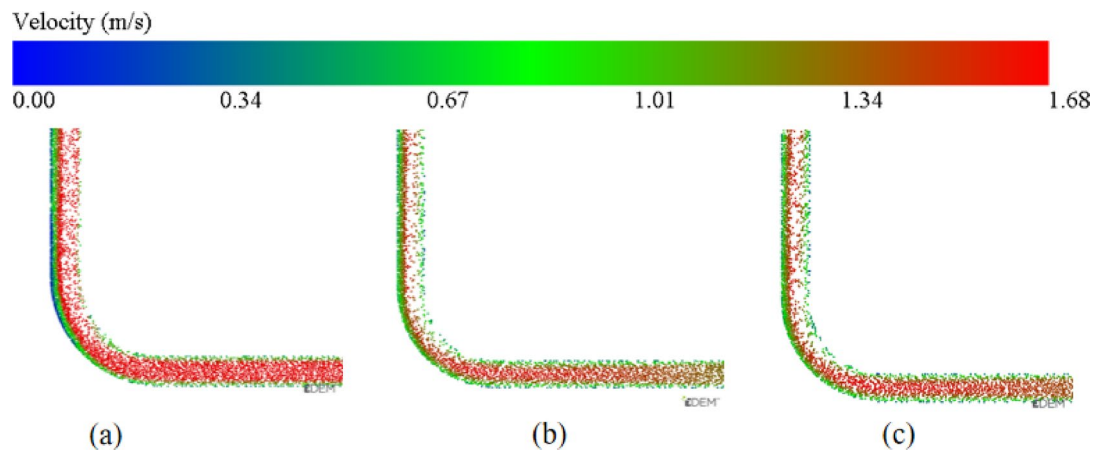

Fig. 9. Particle motion states in the pipeline under different particle diameters: (**a**) D = 2 mm; (**b**) D = 3 mm; (**c**) D = 4 mm.

inner wall pressure. Notably, abrupt directional changes at the bend entrance induce pressure fluctuations, a typical hydrodynamic phenomenon. As flow stabilizes, pressure variations become more regular: lower near the walls and higher at the pipe center. This aligns with Bernoulli's principle, where higher dynamic pressure (from velocity) at the center results in greater total pressure. These insights hold significant implications for optimizing pipeline design and enhancing fluid transport efficiency.

Under the 1.5 m/s inlet velocity condition, comparative analysis of Figs. 7 and 8 reveals a marked shift in particle deposition patterns. At lower velocities, particles predominantly deposit near the inner bend due to weaker centrifugal forces. However, at 1.5 m/s, deposition shifts to the outer bend, demonstrating that higher velocities amplify centrifugal influences, driving particles toward the outer wall. This transition underscores the critical role of inlet velocity in governing particle trajectories and deposition dynamics in curved pipelines.

Influences of particle size on flow
In practical pipeline transport processes, particle sizes are not uniform but exhibit a distribution characteristic. This section investigates three representative particle diameters (d = 2 mm, 3 mm, and 4 mm) under fixed volume fraction (20%) and inlet initial velocity (1.5 m/s). To maintain constant volume fraction, the number of particles entering the pipeline per second increases proportionally with particle size.

Figure 9 details the distribution patterns and velocity characteristics of the three particle sizes. For the d = 2 mm case (Fig. 9a), frequent interparticle and particle–wall collisions due to higher particle influx result in elevated kinetic energy dissipation, reducing the average flow velocity to 0.84 m/s. In contrast, the d = 4 mm case (Fig. 9c) shows increased particle inertia, forming a 1.8 mm-thick deposition band near the inner bend (Table 3) and raising the average velocity to 1.05 m/s (Fig. 10). Larger particles exhibit delayed deposition positions and reduced wall-adjacent sediment volume, indicating improved flowability.

Higher particle influx significantly increases collision frequency, altering trajectories and enhancing kinetic energy dissipation. As shown in Fig. 11a, the temporal velocity profiles reveal this trend. Under the 1.5 m/s initial velocity, the kinetic energy dissipation rate for d = 4 mm particles (16.3%) is 11% lower than for d = 2 mm particles (Fig. 11b and Table 4). The fluid turbulent kinetic energy distribution (Fig. 11d) demonstrates intensified local

Particle diameter (mm)	Deposition thickness at pipe bend (mm)	Pipe pressure drop ΔP (kPa)	Average flow velocity (m/s)
2	5.31	3.56	0.84
3	3.54	3.24	0.96
4	1.86	1.05	1.14

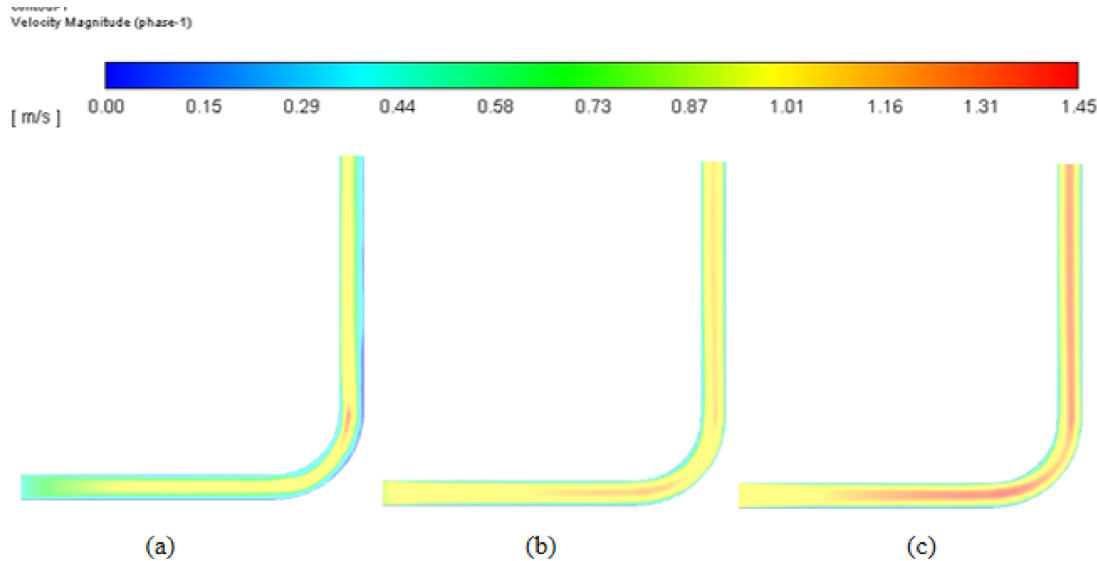**Table 3.** Bend pipe flow parameter comparison.

Fig. 10. Steady-state flow velocity in pipelines with varying particle sizes (**a**) D = 2 mm; (**b**) D = 3 mm; (**c**) D = 4 mm.

turbulence induced by smaller particles, exacerbating energy loss and decelerating particle velocities, reflecting stronger liquid drag and collision interference in small-particle flows.

Pressure, as a core parameter in hydraulic conveying systems of solid–liquid two-phase flow, is closely related to the actual energy consumption in engineering applications. Figure 11c details the pressure drop variations at pipe bend inlets/outlets under different particle sizes. The internal pressure drop of two-phase flow exhibits an intrinsic connection with total energy dissipation, jointly determining the system's energy consumption level. Total energy consumption comprises fluid energy consumption and particle energy consumption. Fluid energy consumption mainly includes energy losses caused by fluid mean velocity, fluctuating velocity, and fluid-wall shear interactions. Particle energy consumption primarily consists of work done to overcome particle gravity, particle–fluid relative motion, and energy dissipation from particle–particle and particle–wall collisions/friction. In horizontal pipelines with stable flow patterns, the work done by particle gravity becomes negligible, while energy dissipation from particle interactions and wall collisions dominates. As particle size increases, the initial injection quantity gradually decreases, leading to reduced interparticle collisions and correspondingly lower kinetic energy loss during particle movement.

The distribution of turbulent kinetic energy within the pipeline warrants thorough investigation. As shown in Fig. 11d, under 4 mm particle size conditions, particles tend to densely deposit at the pipe bottom. This deposition pattern significantly influences turbulent kinetic energy, particularly through particle-induced S_k and S_e influences on turbulence. These influences cause asymmetric turbulent kinetic energy distribution in the pipeline, with the degree of asymmetry progressively intensifying as particle size decreases. The maximum asymmetry occurs at d = 2 mm, reflecting the pronounced influence of small particles on turbulent kinetic energy distribution. During pipeline transportation, the dense particle deposition at the bottom results in higher particle volume fractions significantly affecting local turbulent kinetic energy. With increasing particle size, particle distribution becomes more dispersed, forming a more uniform deposition layer at the pipe bottom. When particle size reaches 4 mm, the reduced initial particle injection quantity and decreased interparticle collisions result in a 69.7% pressure drop reduction compared to the 2 mm case.

Under constant volume fraction and initial inlet velocity conditions, increasing particle size significantly alters particle flow and deposition characteristics within the pipeline. For smaller particles (d = 2 mm), the higher particle count per unit volume leads to dense deposition layers at the pipe bottom, exhibiting a volume fraction approximately 40% greater than that of larger particles (d = 4 mm). Larger particles, due to enhanced inertial influences, demonstrate delayed deposition bed positioning and significantly improved flow uniformity. The increased particle size reduces initial particle injection quantity and decreases interparticle collision frequency, resulting in a total pressure drop reduction of approximately 30%. Energy consumption analysis reveals distinct
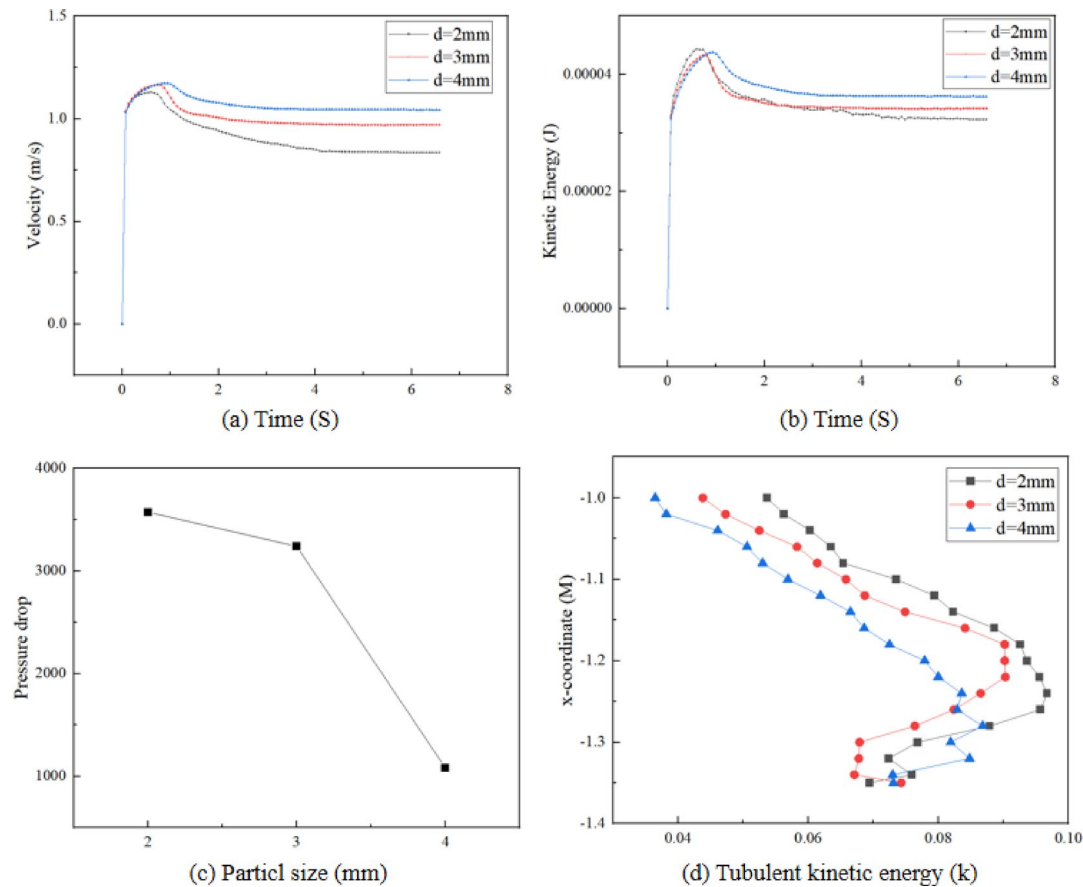
Fig. 11. Influence of particle diameter: (**a**) Velocity variation over time; (**b**) Kinetic energy variation over time; (**c**) Pressure drop versus particle diameter; (**d**) Turbulent kinetic energy variation over position.

Particle diameter (mm)	Kinetic energy peak (J)	Steady-state kinetic energy (J)	Kinetic energy loss rate (%)
2	4.4×10^{-5}	3.2×10^{-5}	27.3
3	4.3×10^{-5}	3.4×10^{-5}	21.0
4	4.3×10^{-5}	3.6×10^{-5}	16.3

Table 4. Influence of particle diameter on energy dissipation.

mechanisms: smaller particles predominantly dissipate energy through interparticle collisions and friction, while larger particles primarily consume energy via fluid shear influences. The high-concentration deposition of small particles at the pipe bottom induces pronounced asymmetry in turbulent kinetic energy distribution, demonstrating that smaller particles exert more intense disturbances on turbulent flow structures.

Influence of irregular particles on flow

In practical pipeline transportation, it is difficult to assume that all particles are spherical. In fact, this study includes two types of irregular particles to analyze the flow dynamics under different velocities. Inlet flow rates of 1 m/s, 1.5 m/s, and 2 m/s were selected to explore the motion characteristics of these irregular particles.

When comparing the deposition under similar velocities, it is clear that irregular particles, especially square particles, show more deposition at higher initial velocities. For example, at a velocity of 1.5 m/s, significant particle accumulation is seen along the curved wall of the pipe. This can adversely affect the regular flow of particles (Fig. 12).

Unlike spherical particles, irregularly shaped particles have more complex geometries, leading to stronger interaction forces per unit volume. Although deposition is minimized at 1.5 m/s, higher inlet velocity result in renewed particle accumulation. This behavior is similar to the deposition patterns seen with spherical particles, where increased flow velocity initially reduces deposition, but beyond a certain critical point, high fluid flow makes particle agitation worse.

As a result, the movement of particles becomes more and more chaotic, leading to a higher frequency of collisions between particles. Under these conditions, elongated particles are likely to have cross-collisions,
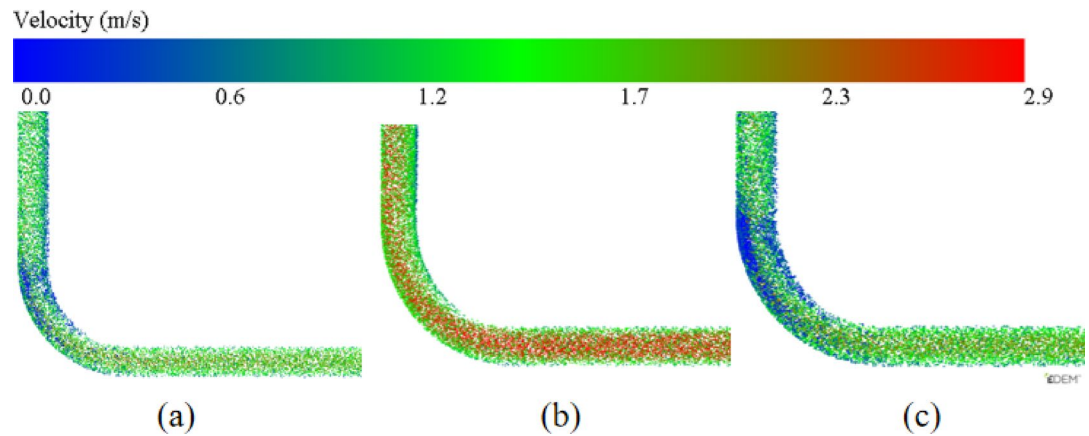
Fig. 12. Square particles motion states in the pipeline under different initial velocities: (**a**) 1 m/s; (**b**) 1.5 m/s; (**c**) 2.0 m/s.
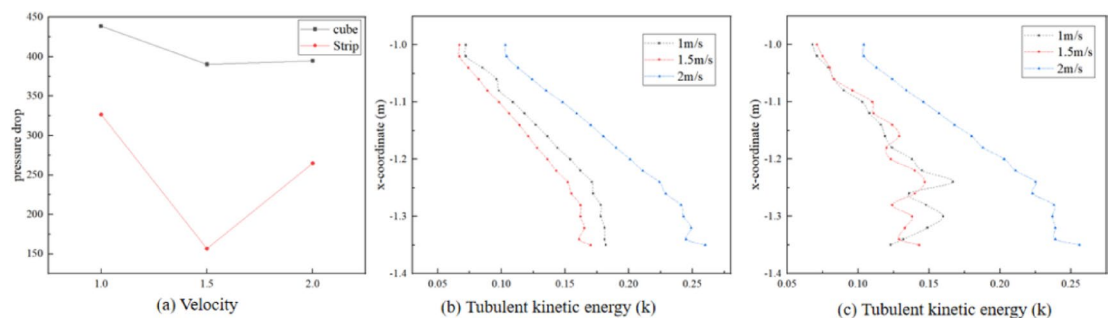

Fig. 13. (**a**) Relationship between pressure drop and velocity; (**b**) Turbulent kinetic energy of rectangular particles; (**c**) Turbulent kinetic energy of square particles.
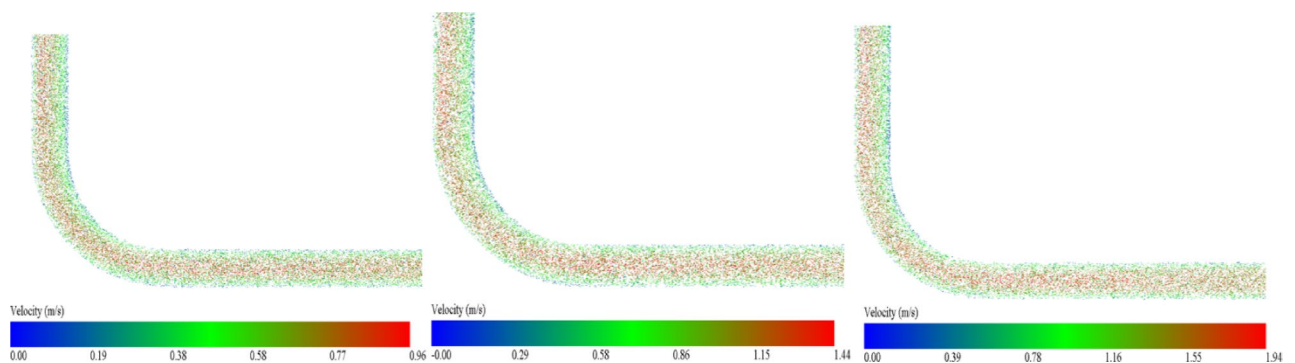

Fig. 14. Rectangular particles motion states in the pipeline under different initial velocities: (**a**) 1 m/s; (**b**) 1.5 m/s; (**c**) 2.0 m/s.

resulting in further accumulation. Eventually, these particles can group together, forming aggregates that contribute to sedimentation inside the pipeline.

As can be observed from Fig. 13a, the intricate shape of square particles causes substantial losses due to collisions and friction with both other particles and the pipe wall, leading to a higher overall pressure drop compared to rectangular particles. Notably, both particle types experience a minimum pressure drop at an initial velocity of 1.5 m/s. Figure 13b,c suggest that the turbulent kinetic energy gradually rises. This is due to the particles settle within the pipeline, which gradually enhances the influence of the source terms S_k and S_ε they generate on the turbulent kinetic energy.

In Fig. 14, particles enter the pipeline through the generation surface and form a small amount of sediment. As the transport speed increases, the flow behavior of rectangular particles starts to resemble that of spherical

particles, changing from an initial moving bed flow to a fixed bed flow. This change indicates that alterations in particle movement patterns mainly result from the unbalanced forces acting on them in different directions, causing a tendency towards sedimentation.

For square particles, when the transport speed is increased from 1 to 2 m/s, they initially move along the bottom inner wall of the pipeline in a pushing manner. However, their unique shape leads to an imbalance of forces in both vertical and horizontal directions, causing their speed to gradually decrease as they travel along the pipeline. In the middle and lower parts of the pipe, the particles tend to almost stop. As the transport volume gradually increases, the stationary particles at the rear begin to accumulate and move forward. Once square particles settle, restarting their movement becomes extremely difficult, resulting in a build-up of particles within the pipeline.

Regarding non-spherical particles like rectangular and square shapes, their flow behavior is inherently more complicated than that of spherical particles. The stronger inter-particle interactions in non-spherical particles increase the frequency of collisions and friction compared to spherical particles. This increased interaction can facilitate settling, especially at higher flow rates or in bends of the pipeline. Moreover, the irregular shapes of non-spherical particles make their movement trajectories less predictable, which can lead to uneven particle distribution and higher risks of pipeline wear and sedimentation. Nevertheless, the influence of flow rate on non-spherical particles is similar to that on spherical particles; exceeding a critical flow rate leads to increased sedimentation within the pipeline. As these non-spherical particles pass through bends, their shape makes them more likely to accumulate against the pipe wall, further compromising transport efficiency.

In this study, a model integrating CFD and DEM was utilized, with sesame seeds as the solid phase and canola oil, which has typical viscous characteristics, as the liquid medium. The emphasis was on probing into the dynamic flow features of food materials within pipelines under different initial velocities, particle sizes, and particle shapes.

When conveying through a bend with an inlet initial velocity of 0.5 m/s, particles tended to pile up in the bend because of gravitational influences. As the inlet velocity rose, this accumulation phenomenon gradually lessened. When the initial velocity reached 1.5 m/s, the faster flow rate led to increased energy losses due to collisions and friction between particles and the pipe walls. Additionally, as the particle size grew, the position of the sediment bed in the bend gradually shifted towards the outlet, reducing the degree of sedimentation, along with a moderate increase in particle velocity. With the increase in particle size, the initial quantity of injected particles decreased, causing a reduction in the interaction forces between particles and the frictional forces with the pipe walls. This reduction ultimately lowered the energy loss of particle motion, resulting in an increase in particle velocity and a alleviation of sedimentation.

For irregularly shaped particles, like rectangular and square particles, their flow behavior in the pipeline is more complex than that of spherical particles. Compared to spherical particles, irregular particles experience stronger interaction forces per unit volume, which raises the frequency of collisions and friction among them. This increased interaction can lead to a higher probability of sedimentation, especially in areas of high flow velocity or curvature. The irregular shapes of these particles also make their trajectories in the pipeline more difficult to predict, which can result in uneven particle distribution and higher risks of pipeline wear and sediment accumulation. However, the influence of flow velocity on the sedimentation of irregular particles in bends is similar to that seen with spherical particles; once the critical velocity is exceeded, sedimentation within the pipeline tends to get worse. The unique shapes of irregular particles may make them more likely to accumulate along the pipe walls, further affecting the transport efficiency.

Figure 15 clearly shows the sedimentation rates at the bends under various transport conditions. The results indicates that, under comparable conditions, the use of rounded particles leads to reduced sedimentation and more stable flow behavior. When adding solids to chili oil, it is advisable to avoid high solid volume fractions. Moreover, adjusting the pumping speed to around 1.5 m/s during the transport process can effectively minimize solid sedimentation within the bends.

To visually illustrate the sedimentation of particles within the pipeline, the calculation of particle sedimentation rate is performed as follows:

$$\eta_d = \frac{M_{total} - M_{wall}}{M_{total}} \qquad (19)$$

where η_d represents the sedimentation rate of particles within the pipeline, M_{wall} denotes the mass of particles at the outlet of the bend, and M_{total} indicates the total mass of particles at the inlet of the bend. Additionally, a fitted curve reveals the relationship between the input initial velocity and sedimentation rate under specific conditions:

$$\eta_d = -0.686^{v/23.263} + 2.681 \qquad (20)$$

where η_d represents the sedimentation rate, and v is the initial conveying velocity.

Although this simulation has identified certain transport patterns, it assumes that the particles have uniform sizes, which does not accurately reflect the complex and diverse nature of solid components in real scenarios. Future work could incorporate simulations of mixed solid particles with varying diameters and densities to better represent the flow conditions in actual products.

It should be clarified that particle "localized particle accumulation" in this study refers solely to mechanical accumulation caused by particle collisions and flow interactions. No cohesive inter-particle forces were included in the CFD-DEM model, thus true cohesive localized particle accumulation was not considered.
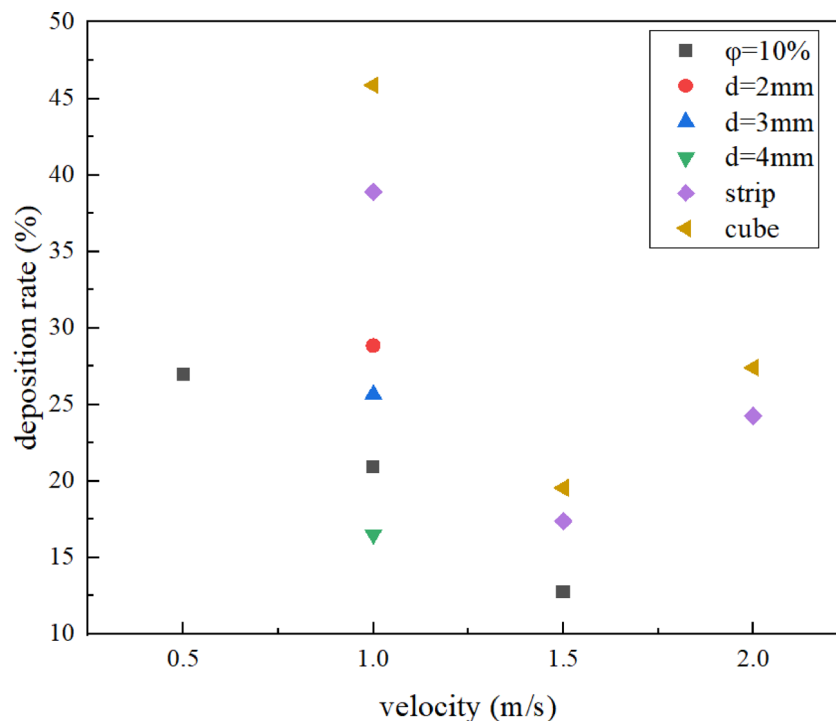
Fig. 15. Relationship between various physical properties and sedimentation rate.

Conclusion

This study establishes a refined CFD-DEM simulation framework to analyze the flow behavior of particle-laden edible chili oil in pipeline bends. The model accurately captures multiphase flow features and matches literature-reported pressure loss data within 8% error, confirming its reliability. The main findings and their implications are summarized as follows:

1. The model exhibits high adaptability across varying inlet velocities (0.5–2.5 m/s) and particle morphologies, accurately predicting key transport parameters such as pressure drop and phase velocities. This provides a robust basis for equipment design and operational control in viscous food-grade fluid systems like chili oil.
2. At low flow rates, particles tend to deposit in the bend due to gravity-induced effects. As velocity increases, deposition is alleviated; however, when the flow rate exceeds a critical threshold (approximately 1.5 m/s), the intensified turbulence and collisions lead to new accumulation zones, particularly along the outer wall of the bend.
3. Larger particle sizes, under constant volume fraction conditions, reduce the number of injected particles. This decreases inter-particle collisions and wall friction, thereby reducing energy losses and increasing transport efficiency. These effects are quantitatively reflected in velocity and deposition trends.
4. Irregular particles, such as rectangular and square geometries, show distinct transport behaviors compared to spherical ones. Square particles, for example, exhibit higher pressure losses (up to 34.56 kPa at 2.5 m/s) due to their unstable orientations and higher surface interaction. While moderate increases in inlet velocity initially reduce deposition, exceeding critical flow rates (above 1.5 m/s) reverses this trend, increasing localized accumulation through intensified cross-collisions and friction.

Overall, this study provides the first quantitative insights into how particle size, shape, and velocity affect pressure drop and deposition in edible chili oil transport. Maintaining inlet velocities within 1.0–1.5 m/s and avoiding high solid fractions is recommended to minimize energy loss and sedimentation. These findings offer direct guidance for optimizing the design and stability of chili oil processing systems.

Data availability

The datasets used and/or analysed during the current study available from the corresponding author on reasonable request. (Jiacheng zhuang,2425169644@qq.com).

References

1. Ranjbari, P. et al. A critical review of the coupled CFD–DEM method for the simulation of two-phase liquid–solid systems. *Powder Technol.* **5**, 454 (2025).

2. Yang, Z. J., Lian, X., Savari, C. & Barigou, M. Evaluating the effectiveness of cfd-dem and sph-dem for complex pipe flow simulations with and without particles. *Chem. Eng. Sci.* **288**, 14 (2024).
3. Shijo, J. S. & Behera, N. Prediction of flow mode transition in pneumatic conveying of fine particles using CFD. *Part. Sci. Technol.* **41**(3), 297–310 (2023).
4. Fang, W., Wang, X., Han, D. & Chen, X. Review of material parameter calibration method. *Agriculture* **12**(5), 706 (2022).
5. Ma, H., Zhou, L. & Liu, Z. A review of recent development for the CFD-DEM investigations of non-spherical particles. *Powder Technol. Int. J. Sci. Technol. Wet Dry Part. Syst.* **412**, 117972 (2022).
6. Nemati, N., Ahangari, K., Goshtasbi, K. & Shirinabadi, R. Optimizing wellbore deviation and azimuth to minimize sand production using a hybrid numerical model in a southwest Iran oilfield. *Geotech. Geol. Eng.* **43**, 1 (2025).
7. Azimifar, M., Moradian, A. & Jafarian, A. A numerical investigation on the dynamics of particle deposition and fouling on a vertical falling film pipe. *J. Water Process Eng.* **66**, 105990 (2024).
8. Qi, Z., Kuang, S. B., Qiu, T. S. & Yu, A. B. Lattice Boltzmann investigation on fluid flows through packed beds: Interaction between fluid rheology and bed properties. *Powder Technol.* **369**, 248–260 (2020).
9. Li, Q. Z. et al. Discrete particle simulation of gas-solid flow in air-blowing seed metering device. *J. Comput. Model. Eng. Sci.* **127**(3), 1119–1132 (2021).
10. Bilal, F. S., Sedrez, T. A. & Shirazi, S. A. Experimental and CFD investigations of 45 and 90 degrees bends and various elbow curvature radii effects on solid particle erosion. *Wear* **476**, 203646 (2021).
11. Chen, L. Y. Numerical simulation of coal water slurry flow characteristics in the inlet section of horizontal pipe. *J. Southeast Univ.* **40**(02), 402–408 (2010).
12. Uzi, A. & Levy, A. Flow characteristics of coarse particles in horizontal hydraulic conveying. *Powder Technol.* **326**, 302–321 (2018).
13. Zhou, M. M. et al. CFD-DEM modelling of hydraulic conveying of solid particles in a vertical pipe. *Powder Technol.* **354**, 893–905 (2019).
14. Dai, Y. et al. Numerical and experimental investigations on pipeline internal solid-liquid mixed fluid for deep ocean mining. *Ocean Eng.* **220**, 108411 (2021).
15. El-Emam, M. A., Zhou, L. & Omara, A. I. Predicting the performance of aero-type cyclone separators with different spiral inlets under macroscopic bio-granular flow using cfd–dem modelling. *Biosyst. Eng.* **233**, 125–150 (2023).
16. Singh, J. et al. Modelling of two phase solid-liquid flow in horizontal pipe using computational fluid dynamics technique. *Int. J. Hydrogen Energy* **42**(31), 20133–20137 (2017).
17. Tian, A., Fu, G., Tang, J. & Wang, D. Numerical simulation of the transport and sealing law of temporary plugging particles in complex fractures of carbonate-type thermal storage. *Energies* **17**(13), 3283 (2024).
18. Peng, Z., Galvin, K. & Doroodchi, E. Influence of inclined plates on flow characteristics of a liquid-solid fluidised bed: A CFD-DEM study. *Powder Technol.* **343**, 170–184 (2019).
19. Chen, X., Yang, L., Luo, L., Yu, L. & Luo, Z. Effects of fluid properties on coarse particles transport in vertical pipe. *Powder Technol.* **449**, 120421 (2025).
20. Sakib, M. N. & Shuvo, M. S. Particle deposition and fluid flow characteristics in turbulent corrugated pipe flow using Eulerian–Lagrangian approach. *Heliyon* **9**(3), 12 (2023).
21. Inthavong, K. et al. A unifying correlation for laminar particle deposition in 90-degree pipe bends. *Powder Technol.* **345**, 99–110 (2018).
22. Li, Z. et al. Flow structure, bed morphology and contaminated sediment transport at the confluences of pipe and channel. *Environ. Fluid Mech.* **24**(3), 367–385 (2024).
23. Vahaji, S., Nguyen, N. H., Shang, Y. & Inthavong, K. Sedimentation effects on particle position and inertial deposition in 90° circular bends. *Powder Technol.* **393**, 722–733 (2021).
24. Lima, V. N., Taheri, A., Randeberg, E. & Skadsem, H. J. Advancements in pipe viscometer system: investigating particle migration effects for enhanced field applicability. In *SPE-Society of Petroleum Engineer*. 000.1–24BERG:13 (2024).
25. Perez, E. L., Asuaje, M. & Ratkovich, N. CFD analysis of counter-rotating impeller performance in mixed-flow pumps. *Processes* **12**(10), 2163 (2024).
26. Qiu, Z., Xiao, Q., Yuan, H., Han, X. & Li, C. Particle shape and clogging in fluid-driven flow: A coupled CFD-DEM study. *Powder Technol.* **437**, 119566 (2024).
27. Crowe, C. T., Sommerfield, M. & Tsuji, Y. *Multiphase Flows with Droplets and Particles* (CRC Press, 2011).
28. Chou, Y. J., Wu, F. C. & Shih, W. R. Toward numerical modeling of fine particle suspension using a two-way coupled Euler-Euler model. Part 1: Theoretical formulation and implications. *Int. J. Multiphase Flow* **64**, 35–43 (2014).
29. Kaushal, D. R., Thinglas, T., Tomita, Y., Kuchii, S. & Tsukamoto, H. CFD modeling for pipeline flow of fine particles at high concentration. *Int. J. Multiph. Flow* **43**, 85–100 (2014).
30. Miedema, S. A. The heterogeneous to homogeneous transition for slurry flflow in pipes. *Ocean Eng.* **123**, 422–431 (2016).
31. Zhao, L. L. Study on the hydraulic transportation mechanism of coarse particles in sand-laden flow in horizontal pipelines. Master's thesis, North China University of Water Resources and Electric Power (2023).

Author contributions

All authors reviewed the manuscript. Jiacheng Zhuang and Qiushi Shi developed conducted measurements, and processed data. Zhi Han supervised, reviewed, and finalized the manuscript, and is responsible for all communication regarding the manuscript.

Funding

Declarations

Competing interests

The authors declare no competing interests.

Additional information

Correspondence and requests for materials should be addressed to Z.H.

Reprints and permissions information is available at www.nature.com/reprints.

Publisher's note Springer Nature remains neutral with regard to jurisdictional claims in published maps and institutional affiliations.